JACS
JOURNAL OF THE AMERICAN CHEMICAL SOCIETY
Cite This: J. Am. Chem. Soc. XXXX, XXX, XXX−XXX
Communication
pubs.acs.org/JACS

Conformationally Induced Off−On Cell Membrane Chemosensor Targeting Receptor Protein-Tyrosine Kinases for *in Vivo and in Vitro* Fluorescence Imaging of Cancers

Yang Jiao,[†,‡] Jiqiu Yin,[‡] Haiyang He,[†] Xiaojun Peng,[†] Qianmiao Gao,[†] and Chunying Duan*[,†]

[†]State Key Laboratory of Fine Chemicals, Dalian University of Technology, Dalian 116024, People's Republic of China
[‡]College of Chemistry, Dalian University of Technology, Dalian 116024, People's Republic of China

Supporting Information

ABSTRACT: Molecules capable of monitoring receptor protein-tyrosine kinase expression could potentially serve as useful tools for cancer diagnosis due to the overexpression of tyrosine kinases during tumor growth and metastasis. In this work, a conformationally induced "off−on" tyrosine kinase cell membrane fluorescent sensor (**SP1**) was designed and evaluated for the detection and imaging of receptor protein-tyrosine kinases *in vivo* and *in vitro*. **SP1** consists of sunitinib and pyrene linked via hexamethylenediamine and displays quenched fluorescence as a dimer. The fluorescence of **SP1** is restored in the presence of receptor protein-tyrosine kinases upon strong interaction with **SP1** at the target terminal. The unique signal response mechanism enables **SP1** use for fluorescence microscopy imaging of receptor protein-tyrosine kinases in the cell membranes of living cells, allowing for the rapid differentiation of cancer cells from normal cells. **SP1** can be used to visualize the chick embryo chorioallantoic membrane and mouse model tumors, suggesting its possible application for early cancer diagnosis.

Tumor formation is always accompanied by blood vessel development and unlimited diseased cell growth. Sunitinib malate is a multitargeted tyrosine kinase inhibitor with antitumor and antiangiogenic activities effective on many tumors, such as breast, lung, prostate and colorectal cancers. Sunitinib malate exerts its antitumor effects by potently inhibiting vascular endothelial growth factor receptor 2 (VEGFR2). VEGFR2, a type of receptor tyrosine kinase, is normally located in the cell membrane. Free circulating VEGFR2 has been evaluated as a surrogate marker for tumor angiogenesis.[1,2] The use of tumor-targeting techniques has rapidly expanded in cancer therapy and visualization.[3−5] Most tumor targets are either membrane proteins or their ligands, which are overexpressed on tumor cells or cancer-associated cells.[6,7] Cancer cells can be labeled by targeting cell membrane receptor proteins, leading to the efficient and early diagnosis of cancer and resulting in early treatment and reduced cancer mortality.[8] Numerous tumor-targeted fluorescent sensors have been reported recently, but only a few target membrane proteins.[9,10]

Compared with conventional techniques, molecular fluorescence imaging has become a powerful tool for targeting membrane proteins and related ligands due to its biological compatibility, high selectivity and high resolution.[11,12] This method has emerged as a promising noninvasive, real-time, high-sensitivity, low-cost technique.[13] Though cell membranes play vital roles in physiological and pathological processes, multicomponent biological complexes make tumor targeting difficult,[14] and long-term debates regarding cell membrane targeting persist.[15] Monitoring VEGFR2 expression *in vivo* and *in vitro* with a small molecular fluorescence sensor could be useful for diagnosis, prognosis assessment, treatment planning, monitoring and research.[16,17] Herein, we designed a receptor-target-based "off-on" fluorescent sensor for the optical imaging of cancer cell membranes, useful in early cancer diagnosis and surgical guidance.[18] It was hypothesized that the fluorescence-quenched sensor **SP1**, a fluorogenic tyrosine kinase inhibitor derivative, migrated across the cell membrane and bound to VEGFR2 inside cancer cells (Scheme 1). The sensor's

Scheme 1. Schematic Diagram of SP1

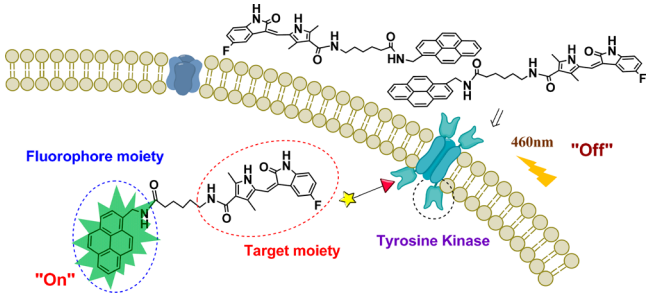

fluorescence signal, which is quenched via the pyrene $\pi-\pi$ stacking interactions, is restored by restraining the conversion of its own configuration due to the push−pull of the associated charge-transfer mechanism. The unique responding mode PET (photoinduced electron transfer) of **SP1** permits the highly selective identification of cancer cells due to a lower background and enables the visualization of cancer-related cell membranes, tissues and a living mouse model, possibly facilitating early diagnoses.[19]

Received: October 10, 2017

DOI: 10.1021/jacs.7b10796
J. Am. Chem. Soc. XXXX, XXX, XXX−XXX

SP1, designed and synthesized in six steps, consisted of three parts: a target group, a linker group and a fluorophore group. The sunitinib target group was synthesized via the Knoevenagel condensation of oxindole and a pyrrolic acid. Sunitinib is expected to target receptor proteins on the cell membrane[20] as it is a multitarget inhibitor of tyrosine kinase. The long aliphatic chain hexamethylenediamine acted as a linker and was connected to sunitinib to improve the biological compatibility of the sensor. The detailed synthetic route and chemical structure of **SP1** are described in Scheme S1. The structure of **SP1** was well characterized by ^{1}H NMR, ESI-MS and 2D NMR analyses. The NOESY spectrum exhibited cross signals between H_a, H_b and H_c of the different pyrene moieties (Figure 1a).[21]

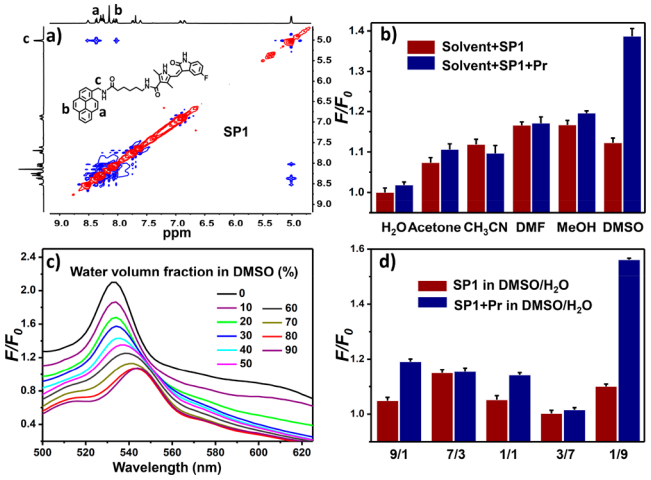

Figure 1. (a) NOESY spectroscopy of **SP1** in a DMSO-d_6 solution. (b) Fluorescence spectra of **SP1** and **SP1**-pr (with the addition of tyrosine kinase) in various solvents. (c) Fluorescence spectra of **SP1** (2 μM) in the DMSO/H_2O medium. (d) Fluorescence spectra of **SP1** and **SP1**-pr (with the addition of tyrosine kinase) in the DMSO/H_2O medium. λ_{ex} = 460 nm. F_0 is the lowest fluorescence intensity of the sensor.

This result suggests that dimeric **SP1** in the free state was stabilized by weak interactions between the two pyrene groups, resulting in significantly decreased background fluorescence and enhanced sensitivity of the sensor.

SP1 (2 μM) showed strong emission in organic solvents, such as DMF, DMSO, MeOH, CH_3CN and acetone, but exhibited weak emission in an aqueous solution (Figure 1b). After the addition of tyrosine kinase, the fluorescence intensity in DMSO exhibited a more significant increase compared with that observed in other solvents. The fluorescence of free **SP1** was quenched upon addition of H_2O to the DMSO solution (Figure 1c). The DMSO/H_2O medium (1:9, 40 mM Tris–HCl, pH 7.4) showed the largest intensity enhancement upon addition of tyrosine kinase and was chosen to simulate biological conditions of the cell membrane environment for the subsequent experiments.

In the DMSO/H_2O simulated physiological medium, **SP1** (2 μM) showed weak emission at 545 nm when excited at 460 nm. Upon addition of the protein-tyrosine kinase receptor (0 to 0.8 μg/mL), an "off–on" fluorescence transformation was directly observed (Figure 2a). The dose-dependent fluorescence enhancement of **SP1** exhibited good linearity with the concentration of the protein-tyrosine kinase receptor in the range of 0 to 0.6 μg/mL, revealing that **SP1** can quantitatively

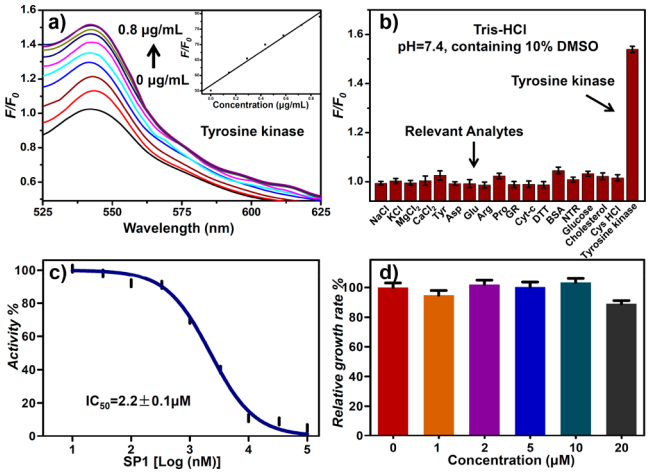

Figure 2. (a) Fluorescence responses of **SP1** (2 μM) to various concentrations of tyrosine kinase. (b) Fluorescence responses of **SP1** to various interferences, including NaCl, KCl, $MgCl_2$, $CaCl_2$, tyrosine (Tyr), glutathione reductase (GR), aspartic acid (Asp), glutamic acid (Glu), arginine (Arg), bovine serum albumin (BSA), proline (Pro), cytochrome C (Cyt-c), dithiothreitol (DTT), glucose, cholesterol, nitroreductase (NTR), cysteine hydrochloride (Cys HCl) and tyrosine kinase. The data were acquired in Tris–HCl (pH = 7.4, 40 mM, containing 10% DMSO). (c) Inhibition of tyrosine kinase by the activity-based probe **SP1**. (d) Relative growth rate (%) of cells that were cultured in the presence of **SP1** (0–20 μM) for 24 h, as estimated by the CCK8 assay.

measure protein-tyrosine kinase receptor levels.[22] Notably, the special two-dimensional structure of the cell membrane makes simulation of the spatial structure and surrounding environment quite difficult.[23] Even though a few studies have used fluorescence techniques to achieve tyrosine kinase detection *in vitro*,[24,25] the linear response of luminescence intensity toward the concentration of tyrosine kinase demonstrated sensitive detection of tyrosine kinase in simulated physiological media.

With tumor growth, the tyrosine kinase receptor VEGFR2 is enriched at the cell membrane surface. The selectivity of **SP1** was investigated in the presence of relevant intracellular substances[26] in the DMSO/H_2O medium. The addition of various amino acids, inorganic salts and other relevant substances had only a slight influence on fluorescence emission (Figure 2b). Furthermore, the IC_{50} (50% inhibitory concentration for tyrosine kinase) was calculated to evaluate the binding capacity of **SP1** with tyrosine kinase (Figure 2c). The IC_{50} value of 2.2 ± 0.1 μM indicated that there is binding affinity between **SP1** and tyrosine kinase. Therefore, **SP1** can selectively target tyrosine kinases over other biologically relevant analytes and selectively label cancer cells. Prior to the bioimaging test, the potential toxicity of **SP1** (0–20 μM) against cancer cells was investigated and the relative cell growth rate was then determined using the CCK8 assay. **SP1** sensor cytotoxicity (Figure 2d and S21) was within an acceptable range, suggesting the biocompatibility of **SP1** in living systems.[27,28]

HT-29 cells, A549 cells and HUVECs are present in human epithelial tissue.[29] VEGFR2 is distributed within these three cell types and is overexpressed during angiogenesis and in cancer cells. Because the probe can recognize the tyrosine kinase receptor, a colocalization assay with D4292 (a commercially available membrane dye) was conducted. HT-29 cells, A549 cells, HUVECs and HeLa cells were incubated with D4292 (1

DOI: 10.1021/jacs.7b10796
J. Am. Chem. Soc. XXXX, XXX, XXX–XXX

μM, green channel) and **SP1** (0.5 μM, red channel) for 30 min (Figure 3a-l). The red channel fluorescence intensities were

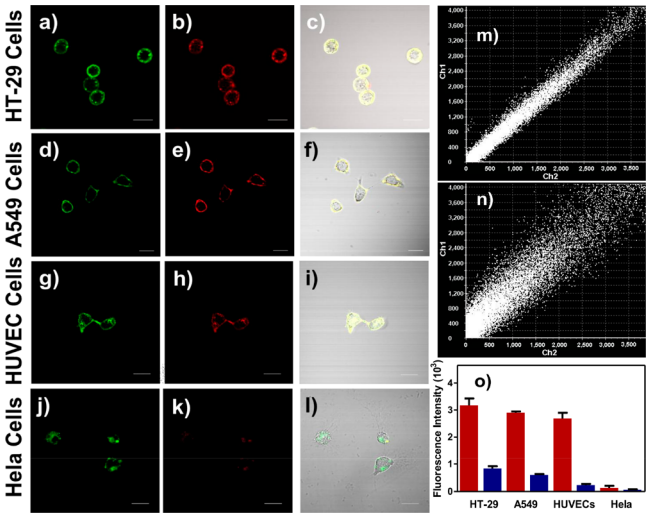

Figure 3. Fluorescence images of HT-29 cells (a–c), A549 cells (d–f), HUVECs (g–i) and HeLa cells (j–l) costained with D4292 (1 μM, green channel) and **SP1** (0.5 μM, red channel). (m) Intensity scatter plot of **SP1** and D4292 in A549 cells (Pearson's coefficient = 0.968). (n) Intensity scatter plot of **SP1** and D4292 in HUVECs (Pearson's coefficient = 0.971). (o) Relative fluorescence intensity in the red channel for the cells. Red bars: Costained with **SP1** (0.5 μM). Blue bars: Costained with **SP1** (0.07 μM). λ_{ex} = 458 nm excitation; λ_{em} = 500–530 nm (green channel) and 530–580 nm (red channel); scale bar = 20 μm.

dramatically higher in HT-29 cells, A549 cells and HUVECs than in HeLa cells. There is a linear relationship of VEGFR2 expression between cells at low sensor concentrations and a good distinction of VEGFR2 expression at high sensor concentrations (Figure 3o). This result suggests that the sensor has good selectivity to target cell membrane of tumor cells and related angiogenic cells.[30]

The commercial dye D4292 and the **SP1** sensor were compared at different concentrations in HT-29 cells. HT-29 cells were prepared by incubation with **SP1** (0.2, 0.5 and 1 μM) for 30 min. With excitation at 458 nm, a bright fluorescence was observed in the red channel (Figure 4b,f,j). The fluorescence of **SP1** overlapped very well with that of D4292 (Figure 4a,e,i) and the Pearson's coefficient was calculated to be 0.99 (Figure 4h). This result implies a preferential distribution of VEGFR2 in the membrane. Fluorescence intensities were enhanced by addition of the **SP1** sensor to HT-29 cells (Figure 4l). The well-matched imaging pattern between **SP1** and membrane dye illustrated the sensor's selectivity toward receptor tyrosine kinases in a biological environment.[31,32]

Angiogenesis plays a key role in the growth of various pathological tissues and is particularly important for biological behaviors, such as the growth and metastasis of solid tumors.[33,34] The applicability of this sensor to deep-tissue imaging in the chick embryo chorioallantoic membrane (**CAM**) with overexpressed tyrosine kinase was investigated. After incubating liver tissue slices from 9-day-old eggs with **SP1** (15 and 25 μM) for 24 h, deep-tissue images were obtained in the same region with excitation at 458 nm (Figure 5). The imaging demonstrated **SP1** visualization of tyrosine kinases in the chick embryo **CAM** with green fluorescence at depths of 0 to 400

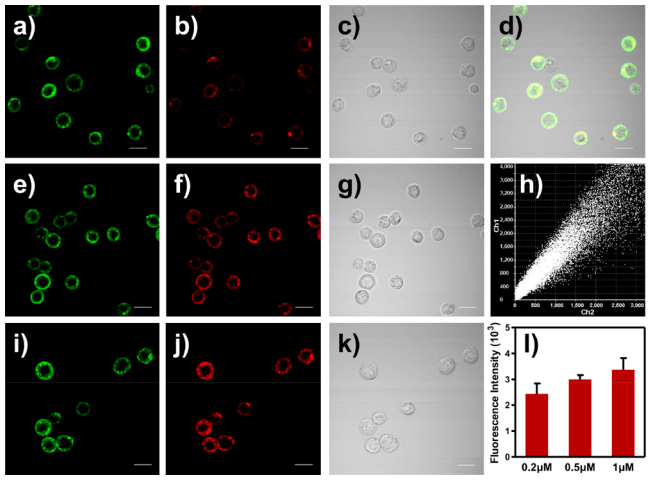

Figure 4. Fluorescence images of HT-29 cells via confocal laser scanning microscopy. (a, e, i) images of D4292; Images of **SP1** at (b) 0.2 μM, (f) 0.5 μM, (j) 1 μM. (c, j, k) Bright-field images. (h) Colocalization coefficient of **SP1** and D4292 in HT-29 cells. (l) Relative fluorescence intensity of the red fluorescence (b, f and j) in HT-29 cells. Scale bar = 20 μm.

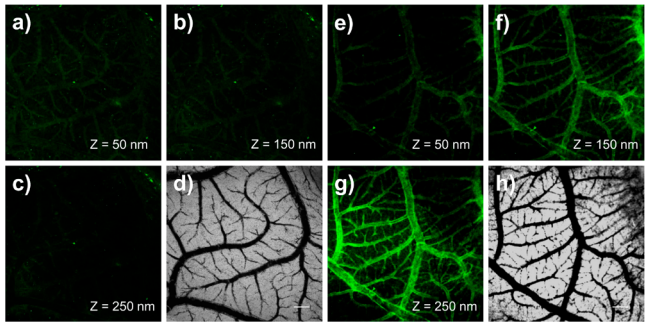

Figure 5. Fluorescence images of the chick embryo **CAM** using **SP1** in 9-day-old fertilized eggs. (a–d) 15 μM **SP1**; (e–h) 20 μM **SP1**. Images were acquired using 458 nm excitation after incubation with **SP1** for 24 h at 37 °C; scale bar = 300 μm.

nm. The results indicated that the sensor can achieve imaging of tissue blood vessels and can be used to monitor effective treatment in tumor therapy.

The *in vivo* fluorescence imaging of tyrosine kinase using **SP1** in a HT-29 tumor-bearing mouse model was further investigated (Figure 6). To determine whether **SP1** can target and monitor tumor cells, varying concentrations of **SP1** were

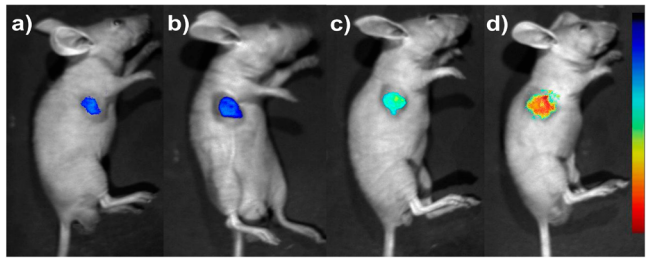

Figure 6. *In vivo* fluorescence imaging of **SP1** in a HT-29 tumor-bearing mouse model via **SP1** injection: (a) 0.1 mM, 100 μL; (b) 0.5 mM, 100 μL; (c) 1 mM, 100 μL; (d) 2 mM, 100 μL. The fluorescence signal was imaged at 500 to 720 nm under excitation with a 460 nm CW laser (power density of 1 mW cm^{-2}).

DOI: 10.1021/jacs.7b10796
J. Am. Chem. Soc. XXXX, XXX, XXX–XXX

directly injected into the tail of mice bearing subcutaneously implanted tumors. Five minutes after injection, strong fluorescence signals were observed at the mouse tumor site and increased with increasing **SP1** concentration (0.1 to 2 mM). Clearly, only the tumor site displayed strong fluorescence images and no fluorescence signal was obtained from other normal organs. These results indicate that **SP1** can be employed for real-time visualization of tyrosine kinases in tumors.[35,36]

In conclusion, we reported the molecular sensor ability of a PET-quenched fluorogenic protein-tyrosine kinase receptor inhibitor. The fluorescence signal is selectively and quickly generated by interaction with protein-tyrosine kinase receptors accumulating on the cell membranes of cancer cells. The "off–on" fluorescence enhancement results from the restrained PET following **SP1** binding to protein-tyrosine kinase receptors on the cell membrane. **SP1** permits the rapid, highly selective and sensitive identification of cancer cells via imaging of the tumor cell membranes, the chick embryo **CAM** and tumors in a mouse model by fluorescence microscopy. Therefore, **SP1** would be useful in the realization of early cancer diagnosis.

■ ASSOCIATED CONTENT

Supporting Information

The Supporting Information is available free of charge on the ACS Publications website at DOI: 10.1021/jacs.7b10796.

Syntheses and characterization of compounds, NMR spectra and MS data (PDF)

■ AUTHOR INFORMATION

Corresponding Author

*cyduan@dlut.edu.cn

ORCID

Xiaojun Peng: 0000-0002-8806-322X

Chunying Duan: 0000-0003-1638-6633

Notes

The authors declare no competing financial interest.

■ ACKNOWLEDGMENTS

This work was supported by the NSFC (Nos. 21501020 and 21421005).

■ REFERENCES

(1) Chang, S. K.; Rizvi, I.; Solban, N.; Hasan, T. *Clin. Cancer Res.* **2008**, *14*, 4146–4153.

(2) Faes, S.; Uldry, E.; Planche, A.; Santoro, T.; Pythoud, C.; Demartines, N.; Dormond, O. *Oncotarget* **2016**, *7*, 1–13.

(3) Yue, Y. K.; Huo, F. J.; Ning, P.; Zhang, Y. B.; Chao, J. B.; Meng, X. M.; Yin, C. X. *J. Am. Chem. Soc.* **2017**, *139*, 3181–3185.

(4) Li, L.; Zhang, C. W.; Ge, J. Y.; Qian, L. H.; Chai, B. H.; Zhu, Q.; Lee, J. S.; Lim, K. L.; Yao, S. Q. *Angew. Chem., Int. Ed.* **2015**, *54*, 10821.

(5) Michaelson, M. D. *Cancer* **2012**, *118*, 1744–1766.

(6) Komatsu, T.; Johnsson, K.; Okuno, H.; Bito, H.; Inoue, T.; Nagano, T.; Urano, Y. *J. Am. Chem. Soc.* **2011**, *133*, 6745–6751.

(7) Kobayashi, T.; Komatsu, T.; Kamiya, M.; Campos, C.; Gonzalez-Gaitáń, M.; Terai, T.; Hanaoka, K.; Nagano, T.; Urano, Y. *J. Am. Chem. Soc.* **2012**, *134*, 11153–11160.

(8) Dai, Z. R.; Feng, L.; Jin, Q.; Cheng, H. L.; Li, Y.; Ning, J.; Yu, Y.; Ge, G. B.; Cui, J. N.; Yang, L. *Chem. Sci.* **2017**, *8*, 2795–2803.

(9) Boonstra, M. C.; de Geus, S. W. L.; Prevoo, H. A. J. M.; Hawinkels, L. J. A. C.; van de Velde, C. J. H.; Kuppen, P. J. K.; Vahrmeijer, A. L.; Sier, C. F. M. *Biomarkers Cancer* **2016**, *8*, 119–133.

(10) Radford, R. J.; Chyan, W.; Lippard, S. J. *Chem. Sci.* **2013**, *4*, 3080.

(11) Li, S. J.; Li, C. Y.; Li, Y. F.; Fei, J. J.; Wu, P.; Yang, B.; Ou-Yang, J.; Nie, S. X. *Anal. Chem.* **2017**, *89*, 6854–6860.

(12) Peng, T.; Hang, C. H. *J. Am. Chem. Soc.* **2016**, *138*, 14423–14433.

(13) Chapin, B. M.; Metola, P.; Vankayala, S. L.; Woodcock, H. L.; Mooibroek, T. J.; Lynch, V. M.; Larkin, J. D.; Anslyn, E. V. *J. Am. Chem. Soc.* **2017**, *139*, 5568–5578.

(14) Lin, W.; Buccella, D.; Lippard, S. J. *J. Am. Chem. Soc.* **2013**, *135*, 13512–13520.

(15) Lee, M. H.; Jeon, H. M.; Han, J. H.; Park, N.; Kang, C.; Sessler, J. L.; Kim, J. S. *J. Am. Chem. Soc.* **2014**, *136*, 8430–8437.

(16) Manning, H. C.; Merchant, N. B.; Foutch, A. C.; Virostko, J. M.; Wyatt, S. K.; Shah, C.; McKinley, E. T.; Xie, J. P.; Mutic, N. J.; Washington, M. K.; LaFleur, B.; Tantawy, M. N.; Peterson, T. E.; Ansari, M. S.; Baldwin, R. M.; Rothenberg, M. L.; Bornhop, D. J.; Gore, J. C.; Coffey, R. *Clin. Cancer Res.* **2008**, *14*, 7413–7422.

(17) Levashova, Z.; Backer, M.; Backer, J. M.; Blankenberg, F. G. *J. Nucl. Med.* **2009**, *50*, 2058–2062.

(18) Patra, M.; Awuah, S. G.; Lippard, S. J. *J. Am. Chem. Soc.* **2016**, *138*, 12541–12551.

(19) Li, Y. H.; Sun, Y.; Li, J. C.; Su, Q. Q.; Yuan, W.; Dai, D.; Han, C. M.; Wang, Q. H.; Feng, W.; Li, F. Y. *J. Am. Chem. Soc.* **2015**, *137*, 6407.

(20) Cella, D.; Davis, M. P.; Negrier, S.; Figlin, R. A.; Michaelson, M. D.; Bushmakin, A. G.; Cappelleri, J. C.; Sandin, R.; Korytowsky, B.; Charbonneau, C.; Matczak, E.; Motzer, R. J. *Cancer* **2014**, *120*, 1871.

(21) Schedlbauer, A.; Coudevylle, N.; Auer, R.; Kloiber, K.; Tollinger, M.; Konrat, R. *J. Am. Chem. Soc.* **2009**, *131*, 6038–6039.

(22) Zhang, H.; Fan, J. L.; Wang, J. Y.; Zhang, S. Z.; Dou, B. R.; Peng, X. J. *J. Am. Chem. Soc.* **2013**, *135*, 11663–11669.

(23) Escribá, P. V.; Busquets, X.; Inokuchi, J.; Balogh, G.; Török, Z.; Horváth, I.; Harwood, J. L.; Vígh, L. *Prog. Lipid Res.* **2015**, *59*, 38–53.

(24) Bai, X. Y.; Huang, Y. Y.; Lu, M. Y.; Yang, D. *Angew. Chem.* **2017**, *129*, 13053–13057.

(25) Lozano-Torres, B.; Galiana, I.; Rovira, M.; Garrido, E.; Chaib, S.; Bernardos, A.; Muñoz-Espín, D.; Serrano, M.; Martínez-Máñez, R.; Sancenón, F. *J. Am. Chem. Soc.* **2017**, *139*, 8808–8811.

(26) Singer, S. J.; Nicolson, G. L. *Science* **1972**, *175*, 720–31.

(27) Zhuang, Y. D.; Chiang, P. Y.; Wang, C. W.; Tan, K. T. *Angew. Chem., Int. Ed.* **2013**, *52*, 8124–8128.

(28) Liu, P.; Calderon, A.; Konstantinidis, G.; Hou, J.; Voss, S.; Chen, X.; Li, F.; Banerjee, S.; Hoffmann, J. E.; Theiss, C.; Dehmelt, L.; Wu, Y. W. *Angew. Chem., Int. Ed.* **2014**, *53*, 10049–10055.

(29) Liu, G. G.; Chen, D. D.; Kong, L. W.; Shi, J. B.; Tong, B.; Zhi, J. G.; Feng, X.; Dong, Y. P. *Chem. Commun.* **2015**, *51*, 8555–8558.

(30) Liu, L.; Liu, X. X.; Xu, Q.; Wu, P.; Zuo, X. L.; Zhang, J. J.; Deng, H. L.; Wu, Z. M.; Ji, A. M. *Int. J. Nanomed.* **2014**, *9*, 3509–3526.

(31) Meng, F. F.; Liu, Y.; Niu, J.; Lin, W. Y. *RSC Adv.* **2017**, *7*, 16087.

(32) Shan, Y. P.; Wang, H. D. *Chem. Soc. Rev.* **2015**, *44*, 3617–3638.

(33) Li, Z.; Qu, T. J.; Ding, C.; Ma, C.; Sun, H. C.; Li, S. R.; Liu, X. H. *Acta Biomater.* **2015**, *13*, 88–100.

(34) Gu, K. Z.; Xu, Y. S.; Li, H.; Guo, Z. Q.; Zhu, S. J.; Zhu, S. Q.; Shi, P.; James, T. D.; Tian, H.; Zhu, W. H. *J. Am. Chem. Soc.* **2016**, *138*, 5334.

(35) Yin, J.; Kwon, Y.; Kim, D.; Lee, D.; Kim, G.; Hu, Y.; Ryu, J. H.; Yoon, J. *J. Am. Chem. Soc.* **2014**, *136*, 5351–5358.

(36) Cheng, D.; Pan, Y.; Wang, Lu; Zeng, Z. B.; Yuan, L.; Zhang, X. B.; Chang, Y. T. *J. Am. Chem. Soc.* **2017**, *139*, 285–292.

DOI: 10.1021/jacs.7b10796
J. Am. Chem. Soc. XXXX, XXX, XXX–XXX